

Landslides (2023) 20:297–313  
 DOI 10.1007/s10346-022-01970-z  
 Received: 13 May 2022  
 Accepted: 31 August 2022  
 Published online: 15 September 2022  
 © The Author(s) 2022

V. Vivaldi · M. Bordoni · S. Mineo  · M. Crozi · G. Pappalardo · C. Meisina



# Airborne combined photogrammetry—infrared thermography applied to landslide remote monitoring

**Abstract** The combination between two remote surveying methods is presented herein as a pioneering approach for landslide airborne monitoring. The survey of an active landslide by UAV-based RGB photogrammetry and infrared thermography, sided by the knowledge of the field condition, allowed increasing the scientific experience on the remote sensing of slope instability phenomena by analyzing multiple aspects related to the evolution of key slope features. In this research, the state and distribution of activity of a landslide was monitored by matching data arising from three-dimensional models of the slope, built by exploiting the aerial RGB photogrammetric technology, and thermal outcomes, resulting from the airborne application of infrared thermography principles. In this frame, thermal anomalies detected during different monitoring campaigns allowed recognizing peculiar features along the unstable slope that could be related to specific kinematic elements involved in the landslide activity. Forming cracks, developing scarps, wet terrain portions, and loose material are some of the elements that could be located by integrating thermal outcomes with Digital Surface Models of the slope. Thanks to the different thermal behavior of such elements, strengthened herein by a novel approach of thermal data processing (i.e. the study of thermal slope profiles), the lateral and retrogressive evolution of the studied movement was first hypothesized and then verified in field. Achieved results show that the location of thermal anomalies well corresponds to field structures, which sometimes are hardly detectable by in situ or RGB surveys, thus suggesting the high potential of the methodological approach developed for this study. The scientific validity of presented data gains relevance thanks to the positive field validation. This paves the way to further studies aimed at implementing the infrared aerial survey of landslides, which surely could bring benefits to practical applications in terms of survey speed and spatial coverage, especially in areas characterized by bad field logistics.

**Keywords** Infrared thermography · Unmanned aerial vehicle · Airborne survey · Landslide · State of activity · Landslide evolution

## Introduction

Landslides are hazardous phenomena which cause significant impacts to people all over the world (Froude and Petley 2018), provoking loss of lives and economic damages, as well as partial or total destruction of environmental settings and human structures (Peduto et al. 2017).

Landslide monitoring is mandatory for hillslope or wide areas affected by slope instability issues, especially when the phenomenon occurrence could determine consequences to elements

at risk located either along the unstable slope or immediately downslope, where the materials mobilized by a landslide could arrive (Corominas et al. 2013). Landslide monitoring allows investigating the kinematic behavior of a phenomenon and the related displacement trends, in order to identify its predisposing and triggering factors, to measure its actual state of activity and possible evolution, and to determine the residual risk in case of an event occurred months or years earlier (Keefer et al. 1987; Yin et al. 2010; Prestininzi et al. 2013; Corominas et al. 2013; Boni et al. 2020; Bordoni et al. 2021; Fusco et al. 2022). All these actions aim to observe the evolution and the possible impact of landslides in susceptible areas, giving also important indications for the development of early warning system strategies and land planning policies to reduce the effects on persons and things (e.g. Alfieri et al. 2012; Pecoraro et al. 2019; Guzzetti et al. 2020).

Landslide monitoring can be performed through various approaches, characterized by peculiar temporal and spatial resolutions (Corominas et al. 2013; Chae et al. 2017). Conventional in situ monitoring techniques (i.e. inclinometers, extensometers, GNSS, topographic leveling, Advanced Differential Interferometric) are widely used to reconstruct and analyze the temporal trends of the displacement and the kinematic behavior of a landslide, both in surface and in deep layers (Petley et al. 2002; Cascini et al. 2014; Intrieri et al. 2019; Liu et al. 2020; Wu et al. 2021). In the latest years, the use of automatic probes, such as inclinometers or GPS systems (Crosta et al. 2014; Vallet et al. 2016; Guo et al. 2019), allowed a continuous monitoring of the evolution of a landslide in field, improving the quantitative analysis, as well as the reconstruction of the evolutionary state (Crosta et al. 2017). However, these techniques can be implemented only in few monitoring points along an unstable slope, limiting the comprehension of complicated and heterogeneous ground motion and kinematic behaviors of large landslides (Chae et al. 2017).

On the other hand, remote sensing techniques, based on terrestrial or air- or space-borne sensors, allow the extensive survey of an unstable area (Bianchini et al. 2021) by acquiring quite spatially continuous data, even with millimetric-centimetric resolution, that can be also integrated with the conventional in situ tools (Canuti et al. 2004; Meisina et al. 2008; Herrera et al. 2013; Raspini et al. 2018; Solari et al. 2019). Nevertheless, remote sensing analysis performed using aerial and satellite platforms show some limitation, mostly related to the high associated costs and the logistical challenge of repeating surveys within a short frequency (Ferretti et al. 2001; Plank et al. 2012).

In this framework, unmanned aerial vehicles (UAVs) are widely spreading to detect and monitor landslides (Giordan et al. 2018,

2020). Compared to other monitoring techniques, UAV-based remote sensing is characterized by real-time applicability at high spatial resolution, together with a relative cheap cost to collect information of wide areas, also in dangerous environments, without risk (Li et al. 2011). The time and cost-effectiveness of this technique allow repeating surveys at regular time intervals according to a continuous monitoring of the changes, related to landslide kinematics and evolution, that occurred between different acquisitions (Giordan et al. 2018).

UAV surveys allow acquiring images, which can be processed to obtain high-resolution topographic data for the reconstruction of landslides morphology and evolution, by exploiting digital photogrammetric techniques (Garnica-Peña and Alcántara-Ayala 2021). Digital photogrammetry, in fact, allows reconstructing topography providing 2D or 3D spatial information from features and elements visible in two or more images acquired from different points of view (Westoby et al. 2012). Once images are oriented and calibrated with field topographic data, it is possible to obtain point clouds, Digital Surface Models (DSM), orthophotos, and 3D representation of objects or surfaces at very high resolution (Colomina and Molina 2014). Different applications of UAVs, equipped with optical cameras to perform digital photogrammetry, have been experienced for mapping and monitoring slope instabilities and their kinematics (Turner et al. 2015; Peternel et al. 2017; Peppia et al. 2017; Rossi et al. 2018; Chudý et al. 2019; Godone et al. 2020; Giordan et al. 2020; Conforti et al. 2020; Mineo et al. 2021; Liu et al. 2021; Nappo et al. 2021). Moreover, the growing use of UAVs for landslide monitoring has led also to new surveying approaches, giving rise to relevant scientific and technical advances. In fact, UAVs can be equipped with multiple sensors operating in different spectral ranges, among which the infrared ones (Giordan et al. 2017; Luo et al. 2020; Melis et al. 2020). With specific reference to the latter, the scientific development of new technologies for the survey of unstable slopes returned satisfactory results with the employment of infrared thermography (IRT). This is a non-contact technique exploiting the capability of every form of matter, with temperature above the absolute zero, to emit thermal radiation (DeWitt and Nutter 1988). It travels in waves with a wavelength between 0.1 and 100  $\mu\text{m}$ , thus mostly falling within the infrared band of the electromagnetic spectrum. Such radiation can be detected and analyzed by thermal cameras, which are capable to convert the infrared thermal radiation into a false color image (Havens and Sharp 2016). According to the Stefan-Boltzmann law, establishing the direct proportionality between the surface temperature of a body and its emitted radiation (Hillel 1998), the surface temperature of an object can be easily estimated through a thermal camera. Thanks to the quick and non-destructive execution of measurements, the use of IRT for remote sensing purposes has rapidly increased. Baroň et al. (2014) used it for mapping open fractures in deep-seated rockslides and unstable cliffs, while Mineo et al. (2015) linked the thermal outcomes surveyed along a weathered rock slope with specific physical features. Literature experiences report IRT among the available technologies for landslide mapping, monitoring, and early warning, even in combination with other surveying methods (e.g. Casagli et al. 2017; Pappalardo et al. 2020; Teza et al. 2012). More specifically, Pappalardo et al. (2018) combined IRT surveys to DInSAR outcomes for the evaluation of the state and distribution of activity of a complex landslide, proving the utility of such approach for

wide areas. Furthermore, several scientific studies are focused on the application of IRT to rock masses, aimed at their geomechanical characterization and thermal monitoring, even in underground environment (Barla et al. 2016; Pappalardo et al. 2016, 2021; Xia et al. 2017; Fiorucci et al. 2018; Guerin et al. 2019; Grechi et al. 2021; Mineo et al. 2022).

The possible integration of thermal sensors with drones paves the way to new possibilities for real-time aerial inspection also applied to landslide analysis and monitoring, coupling thermal measures with more traditional measurements aimed at characterizing landslides from a morphological point of view (Ortiz-Sanz et al. 2019 and references therein).

Based on a study case located along an unstable slope in Oltrepò Pavese area (northern Italian Apennines), where a mass movement was reactivated after its stabilization, this paper aims to present a pioneering methodology to monitor the kinematic behavior and the distribution of activity of a landslide. Starting from the hypothesis that the integration of UAV-based photogrammetry and IRT could provide information on the presence of remotely sensed slope instability-related features, and that the repetition of surveys could shed light on possible evolution of the mass movement, the potential of the multi-temporal airborne IRT application on a landslide area was tested. More specifically, the detection of thermal anomalies associated, both qualitatively and quantitatively, to key elements involved in the evolutionary process of a mass movement was expected by the use of airborne IRT. Furthermore, a detailed three-dimensional model of the unstable slope, where instability elements can be observed and located, is provided for an easier characterization of the studied instability phenomenon. Finally, the monitoring challenge by UAV-based photogrammetry and IRT is pursued herein by integrating data collected in the same period to achieve matched information on morphological evidences of landslide activity, kinematics, and distribution of activity.

### The studied landslide

The studied landslide is located close to the Ghiaia dei Risi village (44°58'11.89" N–9°09'28.30" E), in the Oltrepò Pavese hilly zone (northern Italian Apennines, north-western Italy; Fig. 1).

The slope instability phenomenon affects a north-western facing hillslope with limited length (about 90 m), covered by woods and shrubs, at altitude between 229 and 147 m above sea level (a.s.l.). Slope angle increases along the hillslope, passing from 8–12° in the highest sector (above 200 m a.s.l.) to 18–20° in the low-lying part (below 200 m a.s.l.).

From the geological point of view (Meisina et al. 2006), the unstable hillslope is characterized by a bedrock composed by marls and sandy marls belonging to eocenic-miocenic deposits of Antognola Marls and Ranzano Formation. Marley bedrock is in contact with claystones and clayey melanges with a block-in-matrix texture of in the highest part of the hillslope. Dormant slow-moving landslides, mostly rotational/translational slides and rotational slide evolving in flowslide (Cruden and Varnes 1996), developed in 1970s are present in surrounding hillslopes, confirming the significant proneness of this territory to this type of slope failures. The test-site and the surrounding slopes belong to the catchment formed by Ghiaia di Montalto creek, whose quaternary alluvial deposits (mixture of sand, silt and clay) are present at the foot of the studied hillslope.

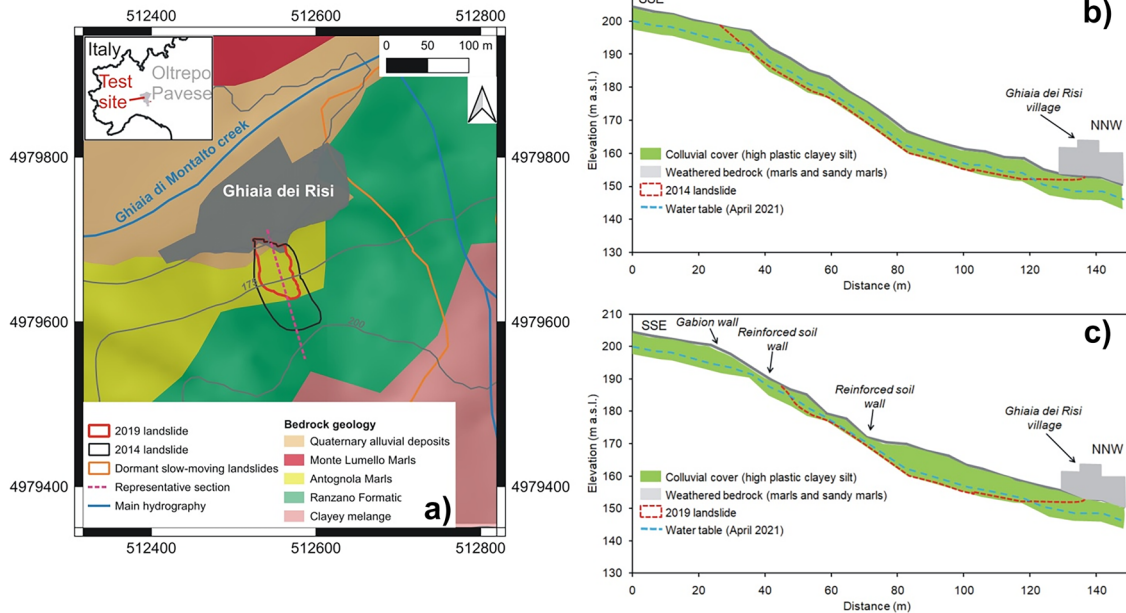


**Fig. 1** Test-site location (the map is projected in WGS84-UTM Zone 32 N) and main settings (a). Representative section along the slope, after the landslide event of 2014 (b) and of 2019 (c)

A homogeneous colluvial cover is present above bedrock materials of the unstable slope (Fig. 1), whose main physical and geotechnical features are summarized in Table 1. The following laboratory tests were carried out on representative samples of the test-site according to the American Society for Testing and Materials (ASTM): (i) grain size analyses and Atterberg limits on disturbed samples; (ii) drive-cylinder method for the measure of volumetric features of undisturbed samples.

Colluvial cover develops in depth as deep as the contact with the weathered bedrock at about 4.8–6.6 m b.g.l. Its clayey silt texture is characterized by high plasticity (CH, according to Unified Soil Classification System). Unit weight is low (17.1–17.8 kN/m<sup>3</sup>), confirming it is a soft colluvial cover. Below such cover, weathered bedrock is composed by marls and sandy marls, with local levels of claystones. A more compact marly bedrock is located at 4.8–7.8 m b.g.l., according to boreholes data and static penetrometric tests carried on October 2016 and to dynamic penetrometric tests and 2D-refraction seismic profiles carried on April 2021. The contacts between these layers are located at quite steady depths along the hillslope, following the ground surface trend (Fig. 1).

A water table is present in the deepest horizons of the colluvial cover, above the contact with the weathered bedrock, typically at depths between 4 and 6 m b.g.l. (Fig. 1). However, the water table

can rise up to the shallowest horizons in correspondence of significantly rainy periods.

The test-site slope experienced two main triggering events in the past 7 years. The landslide was triggered for the first time in winter 2014, after an important rainy period occurred between January and the beginning of March 2014. This landslide was 5,743 m<sup>2</sup> wide involving the medium-terminal part of the hillslope (Fig. 2).

After this event, several remediation works were carried out on 2017 to reduce the susceptibility of the area. These were constituted by a set of gabion walls built at the top of the hillslope, at the source area of 2014 landslide, and by two reinforced soil walls built perpendicular to the slope direction, at two different parts in the middle area of the hillslope, and provided of drainages at their basis to allow the shallow water flows (Fig. 3a).

A remarkable reactivation of the landslide occurred in the significant rainy period between November 2019 and January 2020. The reactivation occurred again in the medium-terminal part of the hillslope, involving in particular the central and the terminal parts of the 2014 slope failure. The reactivation, covering a 2500 m<sup>2</sup> wide area, caused the partial collapse of one reinforced soil wall. After this event, some superficial drainages were built to help in removing part of the shallow water from the unstable area and carrying it to the deep drainage system at the basis of the hillslope.

**Table 1** Main physical and geotechnical features of the colluvial cover involved in the slope instability

Depth (m)	Gravel (%)	Sand (%)	Silt (%)	Clay (%)	w <sub>L</sub> (%)	P <sub>I</sub> (%)	USCS	γ (kN/m <sup>3</sup> )
0.0–6.6	0.1–5.0	0.9–2.0	60.5–63.9	32.5–35.1	55.3–56.0	32.6–33.0	CH	17.1–17.8

w<sub>L</sub> liquid limit, P<sub>I</sub> plasticity index, USCS Unified Soil Classification System, γ unit weight, CH clay of high plasticity

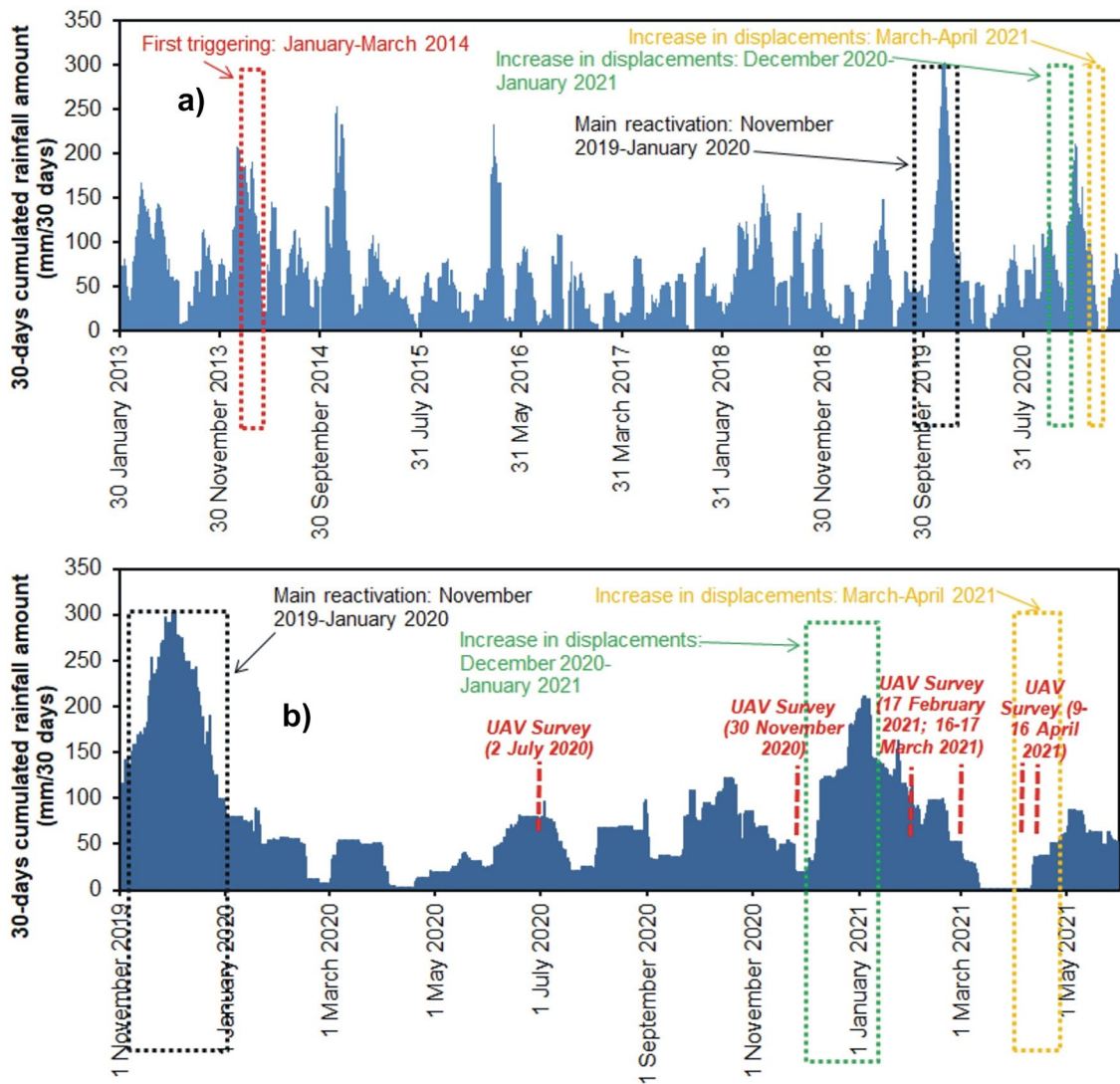


**Fig. 2** **a** 30-day cumulated rainfall amount measured in the period between 1 January 2013 and 21 May 2021 in correspondence of FRG. **b** Detail of the 30-day time series of cumulated rainfall amount measured

in the period between 1 November 2019 and 21 May 2021 with indication of UAV and field surveys

This system of drainages was 0.2–0.5 m deep and was composed by a main drainage, running parallel to the slope gradient immediately above the damaged reinforced soil wall, and by other shallow drainages with NW–SE direction.

Landslide reactivations occurred during prolonged rainy periods, suggesting a triggering role for rainfalls. The triggering of the first landslide and its main reactivation occurred when 30-day cumulated rainfall amounts counted over 180 mm, as occurred in February 2014 (peak of 185.8 mm/30 days on 11 February 2014), November 2019 (peak of 297.6 mm/30 days on 27 November 2019), and December 2019 (peak of 303.8 mm/30 days on 2 December 2019), according to Fortunago Rain Gauge (FRG) belonging to Arpa Lombardia monitoring network (located 7 km away from the test-site, at 500 m a.s.l.) (Fig. 2).

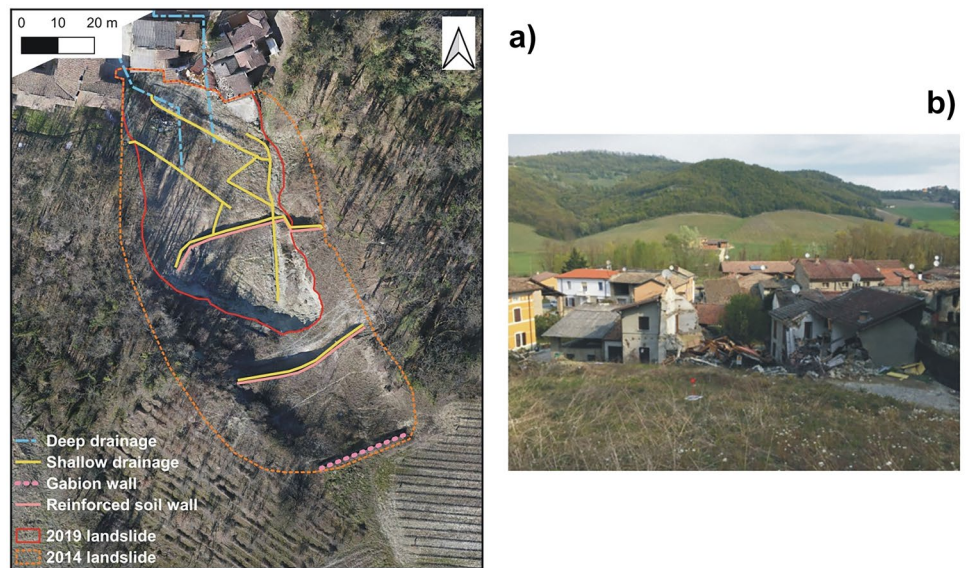
The first landslide and its reactivation developed along a sliding surface located at about 6 m b.g.l., at the contact between

colluvial cover and weathered bedrock. Such mass movement can be classified as a complex landslide, formed by a rotational slide that evolves in a flow-slide at its terminal part (Cruden and Varnes 1996).

The displacements induced by the November 2019–January 2020 reactivation increased from December 2020 to January 2021, as testified by a progressive formation of new fractures and an enlargement towards lateral and upslope directions. December 2020 was significantly rainy, with a peak of 192.8 mm/30 days on 30 December 2020 (FRG), as it occurred when the slope first failed in 2014 and then in 2019 (Fig. 2).

Furthermore, after the rainfall events between March and April 2021, characterized by a peak of 37.2 mm of rain fallen in 30 days (FRG), new N-S oriented cracks developed beyond the lateral limits of the landslide, while an E-W trending crack formed over its crown (Fig. 3). During this last rainy period, water table

**Fig. 3** The studied landslide at March 2021: **a** orthoimage of the unstable slope, with boundaries of 2014 and 2019 landslides and the remediation works carried out on the hillslope; **b** damages to the buildings located downslope immediately below the landslide



laid at 2.5–4.0 m b.g.l., according to measurements performed at boreholes located at the foot of the unstable slope.

The displacement induced by this landslide is causing progressive and significant damages to the buildings located downslope, with the partial or total collapse of several parts of the houses located immediately below the landslide (Fig. 3).

#### Data and methods

The landslide investigation was performed by involving different types of input data and survey techniques (Fig. 4).

The interpretation of satellite images acquired at different periods presented in Google Earth Pro was the first step to reconstruct the landslide displacements after the first 2014 triggering event and during the main reactivation phase in 2019.

Different satellite acquisitions were analyzed to map the landslide evolution. These refer to 29 May 2012 (before all events), 23 October 2015 (after the first triggering event), 30 March 2017 (after the remediation works), and 10 April 2020 (after the reactivation of November 2019–January 2020) (Fig. 5). In this step, the area progressively displaced by the 2014, 2019, and 2020 events was mapped.

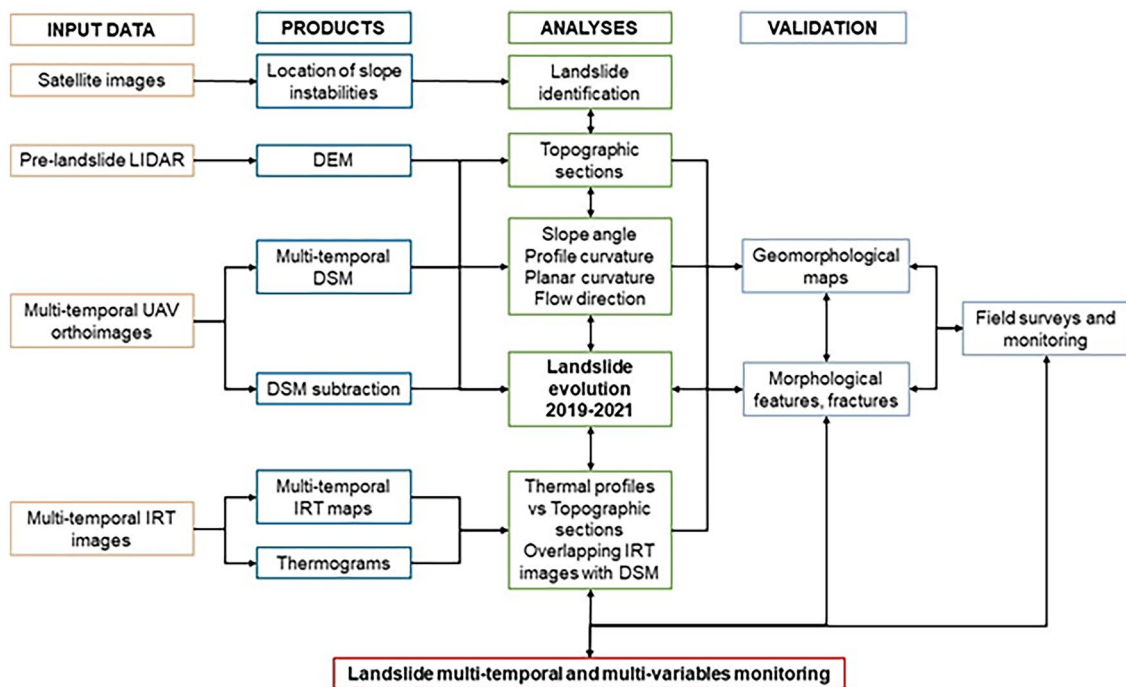


**Fig. 4** Flowchart of the work method

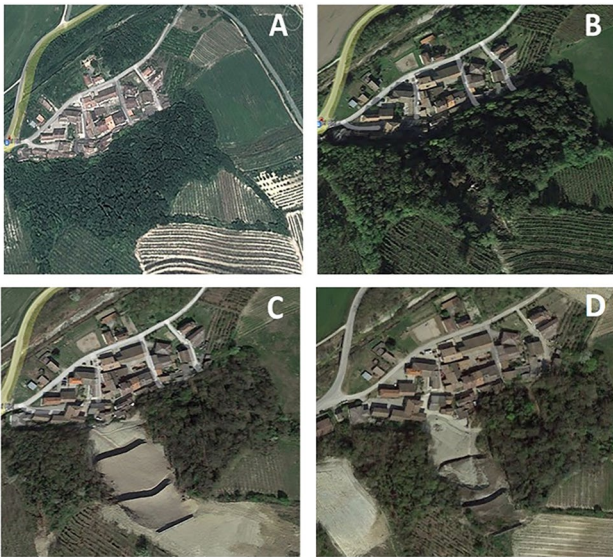


**Fig. 5** Landslide evolution from 2012 to 2014 from Google Earth Pro. **A** Image acquired on 29 May 2012 before landslide triggering; **B** image acquired on 23 October 2015 after the first triggering event; **C** image acquired on 30 March 2017 after the slope safety works; **D** image acquired on 04 October 2020 after the second triggering event

The so determined unstable area was set as “*time 0*” for the following multi-temporal landslide monitoring.

Using the regional 1 m/px Digital Elevation Model (DEM) retrieved from LiDAR data acquired in 2008 and 2010 by the Italian Ministry for Environment, Land and Sea, within the framework of the “Extraordinary Plan of Environmental Remote Sensing” (PST-A), morphological parameters such as *slope angle*, *profile*, and *planar curvatures* and slope orientation (*aspect*) were

derived to enlighten the slope morphology occurring before the first landslide triggering event. Morphological parameters were calculated in GIS software environment, by using SAGA GIS and *Quantum GIS*, and their associated rasters were classified and vectorised using ESRI Arc Map.

UAVDP (unmanned aerial vehicle digital photogrammetry) surveys were carried out to monitor the landslide evolution in time, providing different kinds of multi-temporal data. Such surveys were performed in 6 different times, in order to retrieve high-resolution orthoimages and Digital Surface Models (DSMs) in different periods and to monitor the landslide activity both throughout about 1 year of observation and during different phases of its kinematic evolution. The UAV data acquisition was scheduled as follows: 2 July and 30 November 2020, after the reactivation of November 2019–January 2020; 17 February and 16–17 March 2021, after a second reactivation occurred in December 2020–January 2021; 9 and 16 April 2021, to monitor the kinematic evolution of the displacements during the last period of the monitored time span.

A mirrorless Sony ILCE-6000 24 Megapixel camera (APS-C sensor) (Sony Europe Limited) with 16-mm lens and a thermal camera Flir Vue Pro R with 13-mm lens were mounted on a hexacopter (UAV) using a 3-axis gimbal (Fig. 6a). Main specifications of UAV and camera are reported in Table 2.

The UAVDP surveys were conducted with a nadir orientation of the on-board cameras and the acquisition of digital photographs with a minimum overlap and side-lap of about 85% and 80%, respectively. In order to capture the complex geometry of the area (Fig. 6b) and to improve the accuracy of the generated model, the images were acquired from parallel positions (strips of photographs taken along a fly line). The distance between the camera and the terrain surface was about 50 m. Ground Sample Distance (GSDs) was kept constant during the mission and the flight plan was based on a DTM extracted from a previous UAV survey of the entire basin. UAV was flown under automatic

**Fig. 6** UAV with infrared camera employed for this work (a). UAV survey flight area (b). Mission flight of each UAV survey (c)

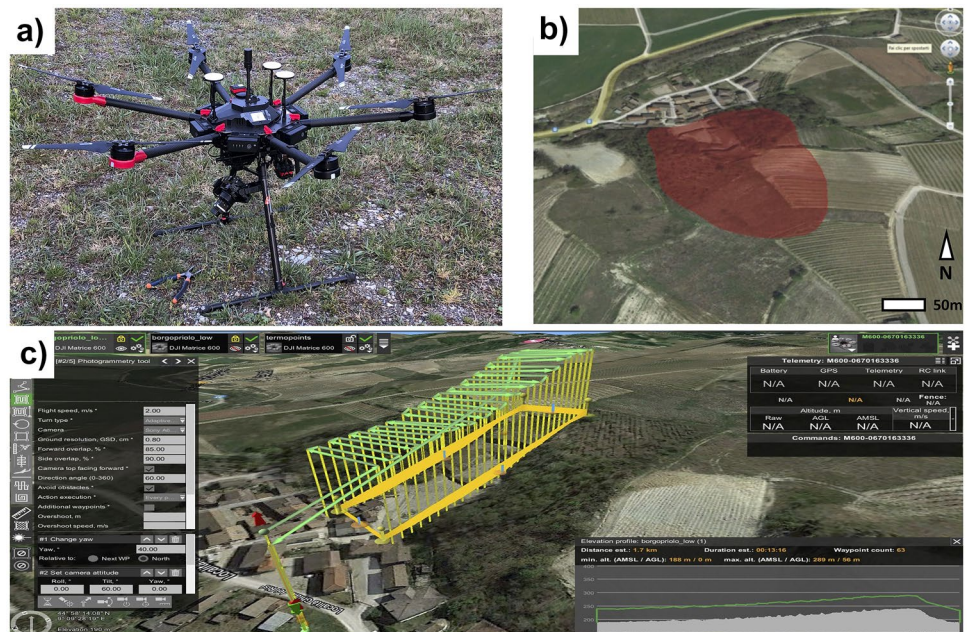


**Table 2** UAV and UAV camera specifications

UAV type	Diameter	Engines	Rotor diameter	Empty weight	UAV autonomy
Djimatrice 600 Pro	167 cm	Brushless	21 in. (53.34 cm)	5.9 kg	38'
RGB camera	Sensor type	Sensor size	Image size	Pixel size	Focal length
Sony 6000 ILCE	APS-C	23.5 × 15.6 mm	6000 × 4000 px	3.92 × 3.90 μm	28 mm
Thermo camera	Spectral band	Sensor size	Image size	Pixel size	Focal length
Flir Vue Pro R	7.5–13.5 μm	10.88 × 8.704 mm	640 × 512 px	17 × 17 μm	13 mm

control in a sequence of left-and-right flight lines covering the full vertical extent of the area (Fig. 6c).

All photographs were georeferenced and oriented by the UAV on board GNSS/IMU instrumentations and Post Processing Kinematic (PPK) differential GPS system, with a horizontal mean error of 1.7 cm and a vertical mean error of 3.2 cm.

During all the UAV surveys, Digital Surface Models (DSMs) were retrieved and processed to obtain the main morphological attributes of the slope (slope angle, profile and planar curvatures, slope aspect) and their evolution in time. Furthermore, DSMs were processed by using mathematical difference, in order to reveal potential landslide displacements occurring between two or more consecutive surveys. UAV surveys provided 4 DSM and orthoimages acquired in 4 different times, during the monitoring period (2020–2021). From such models, morphological parameters, such as the slope angle, profile and planar curvatures, flow direction, and hillshade map were extracted.

In addition to the RGB images, UAV provided also IRT images of the area, allowing a thermal analysis of the landslide. Thermal cameras allow the non-contact estimation of the surface temperature of framed subjects, resulting in the possibility of mapping the temperature variations within a specific area. Therefore, IRT surveys are useful to detect specific features hardly visible to the naked eye or on RGB images (e.g. cracks, fractures, wet areas). IRT data were collected during the UAV surveys of 16–17 March, 9 April, and 16 April 2021, after both the second reactivation of December 2019–January 2020 and the kinematic evolution of the landslide in March–April 2021.

The acquisition of thermograms was performed both before dawn and after sunset, in order to reduce as much as possible the contribution of the solar radiation leading to shadow effects and non-uniform surface heating. In fact, dark conditions proved the best setting for a good detection of fractures, cracks, and wet areas (e.g. Mineo et al. 2015; Pappalardo et al. 2016). The RGB camera and the thermal camera has identical FOV (field of view = 45°), but different resolutions (0.7 cm/px for RGB e 6.53 cm/px for thermal). The thermal survey planning was different from the RGB one; the drone flight plan had less waypoints and a different relative height; furthermore, the yaw and pitch are not fixed to fit the morphology area.

Resulting thermal images were post-processed to find the best balance between displayed surface temperatures and slope features. Emissivity was set to 0.93, corresponding to a representative value of soil (between saturated and dry), according to FLIR (2017) and some literature experiences (e.g. Pappalardo et al. 2018). Thermal images were then analyzed and some key features linked to the

instability process were highlighted. Moreover, a pioneering analysis of the landslide was carried out on thermograms by defining thermal profiles along specific slope sections. Such profiles highlighted the spatial location of some key thermal peaks, which were compared to the location of instability features, surveyed both in field and on RGB models, and to the corresponding topographic section. IRT images were then overlapped to the corresponding DSM, achieving a clear match between the employed technologies and validating their combined use.

On the other hand, field surveys allowed a detailed mapping of the features related to the landslide evolution: fracture opening and orientation were measured in all surveys, in order to detect possible evolution of the landslide. Field surveys were carried out on 24 February and 2 July 2020 to observe the main morphological features and the effects induced by the displacement in the unstable area of November 2019–January 2020. Moreover, a further field survey was performed on 16 April 2021, to verify the results of UAV data analyses and to quantify the effects of the displacements induced by the reactivation occurred in December 2020–January 2021 and by the increase in ground motion that occurred on March–April 2021.

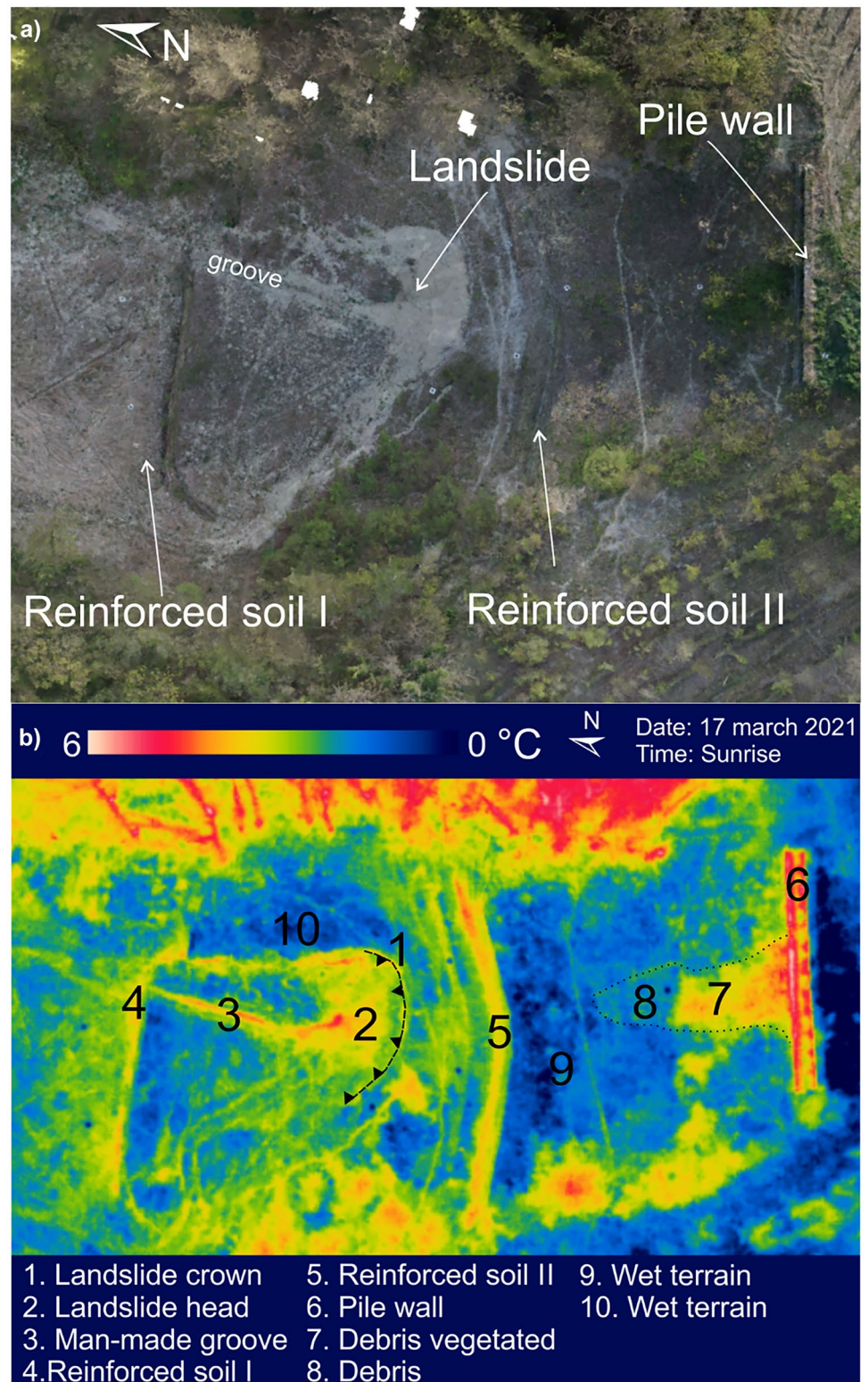
All the identified features were traced and mapped through a high-resolution GPS and vectorised into Esri shapefile to map their possible evolution. The results of field surveys, together with the geomorphological attributes observed through UAV surveys and the corresponding effects on IRT images, allowed validating the photogrammetric and the IRT products. In this way, a monitoring of the landslide activity and evolution up to the end of May 2021 was performed integrating multi-temporal and multi-variables products.

## Results and interpretation

### Analysis of thermograms

The analysis by IRT was carried out by taking into account thermograms referring to different monitoring campaigns, which were herein compared to shed light on the main features characterizing the movement. The general infrared frame of the area (Fig. 7), captured on 17 March 2020, returns an overview of thermal anomalies defining both the landslide and the stabilization structures built in 2017. In particular, the landslide crown is highlighted by a circular positive anomaly rimmed, to the north, by a circular warmer sector suggesting a sort of ground sinking. This corresponds to the landslide head, where a marked linear positive anomaly affects the landslide body. It is a man-made groove running as far as the breach in the downstream order of reinforced soil caused by the landslide itself. In the upper sector, the second order of reinforced soil and

**Fig. 7** **a** Aerial photo of the area framed by IRT in inset **b**; **b** infrared overview of the landslide area with the main recognized elements reported



the pile wall on the top are marked by positive, continuous anomalies. In the latter case, the highest surface temperatures are found at the central portion of the pile wall, testifying a sort of undercutting. This is strengthened by the presence of loose material accumulated

along the slope and labeled by intermediate surface temperatures thanks to the presence of vegetation. In fact, in such specific time conditions (before sunrise), vegetation proved gaining higher surface temperature than the colder soil. Below the vegetated debris



body, a slight positive thermal anomaly suggests the presence of a further debris front, probably arising from washout phenomena affecting the upstream debris accumulation. Finally, the presence lowest surface temperature zone right behind the second order of reinforced wall and on the eastern margin of the landslide suggests a possible concentration of ground humidity, thus the presence of local wet terrain portions, even considering that no rainfall occurred in the previous days and that some drainages are present in the upper slope portion.

For a better analysis of the landslide depletion zone (Fig. 8a), aimed at finding out possible evidence of peculiar evolution features, thermograms acquired during different surveys are herein compared (Fig. 8b–d). In particular, a frame taken on 16 March 2021 at sunset (Fig. 8b) shows that the crown is marked by a positive anomaly making easy its infrared recognition. At the upper part of the main scarp, both to the east and to the west, some warm alignments suggest the presence of cracks whose opening rate is supported by the higher temperatures. At the time of this survey, the sunset thermogram suffers from the influence of a residual solar radiation, resulting in a differently lightened scarp. Nevertheless, the presence of loose material, partly mobilized along the eastern flank of the landslide, is highlighted by the marked positive anomalies related to an evolution of the scarp. On the western flank, the

presence of tension cracks, suggesting an ongoing enlargement of the movement, is testified by positive linear anomalies. Finally, a slight positive anomaly upstream of the crown, with a semicircular shape, is recognized at a morphological step surveyed on the ground.

The thermogram related to sunrise condition (Fig. 8c), acquired the day after, shows that the main scarp is labeled by intermediate surface temperatures and the man-made groove is marked by the highest temperatures. Opened cracks are detected by positive linear anomalies at both the crown edge and at the western sector, where a retrogressive scarp is forming. The interesting information is that a slight positive anomaly, which was not detected at sunset, crosses the eastern sector of the area and connects to the crown. This can be hypothesized as the evidence of a landslide lateral evolution. One month later, on 16 April 2021 preceded by rainfall days, the best IRT outcomes are found by constraining the surface temperature range within a narrow interval (Fig. 8d). In this case, the developing eastern cracks are marked by positive anomalies, even suggesting a sort of opening degree. The slope portion enclosed between such cracks and the landslide scarp can be therefore referred to as a potential enlargement sector of the landslide itself. Similarly, on the opposite flank, the forming scarp previously highlighted is herein labeled by a negative anomaly, suggesting a more exposed sub-vertical surface

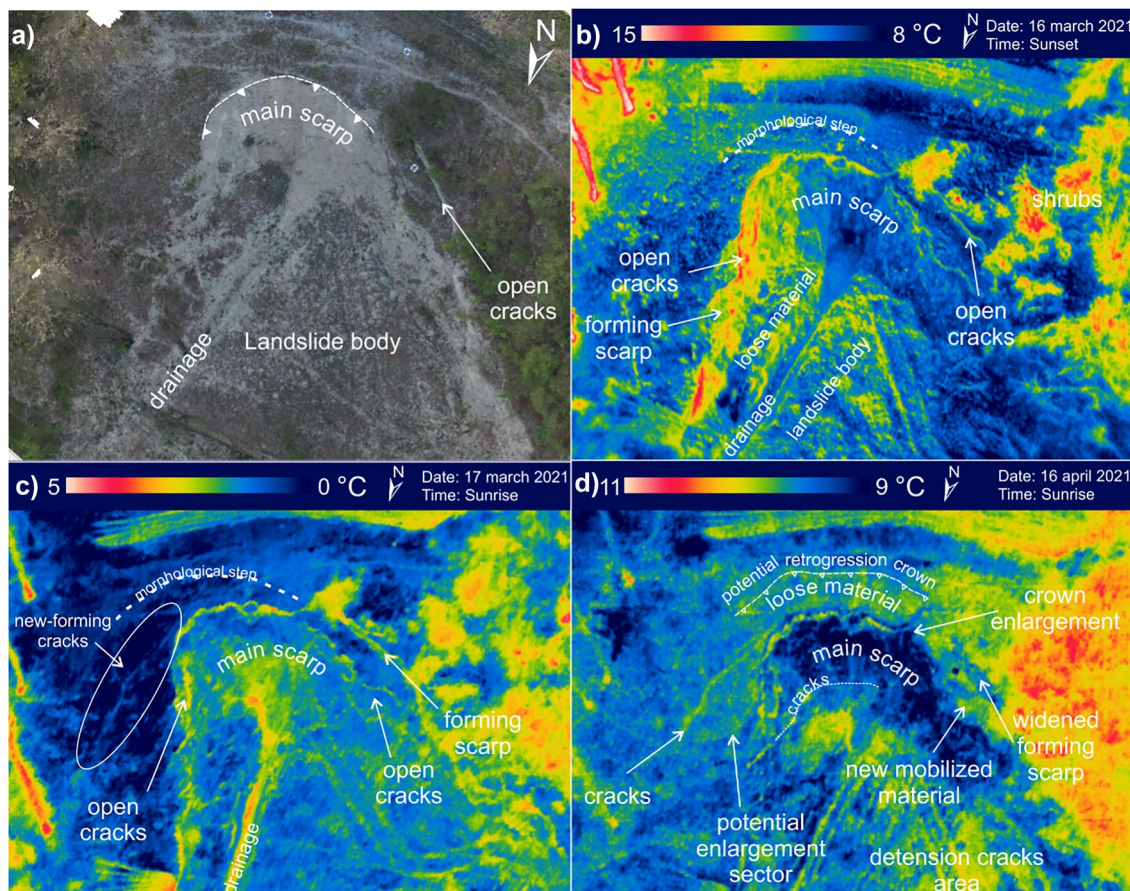


**Fig. 8** a Aerial photo of the area framed by IRT in insets b–d; b focus of the landslide depletion zone taken late in the evening on March 2021; c focus of the landslide depletion zone taken early in the morning

ing on March 2021; d focus of the landslide depletion zone taken early in the morning on April 2021

proving its widening in only 1 month. The landslide crown shows also signs of lateral evolution, with head cracks connecting to the aforementioned western scarp, thus allowing the identification of new mobilized material. The morphological semicircular step upstream of the crown is more evident, thus becoming a true potential sign of a retrogression crown. Moreover, the lowest temperatures found at the main scarp could be the result of subsoil water circulation, probably enhanced by the previous rainfalls, which likely flows on the landslide body following the drainage direction. Within such a cold sector, at the lower portion of the main scarp, slight positive thermal anomalies are aligned testifying the presence of cracks, likely due to the progressive detension caused by the sliding of the landslide head. Finally, the positive thermal anomaly occurring at the lowest sector of the landslide body (Fig. 8d) is likely related to a concentration of detension cracks.

### Digital Terrain Model analysis

The analysis of multitemporal DSM was carried out by calculating the differences between the oldest model (2020) and the more recent one (2021), in order to highlight the landslide evolution during the monitoring period.

The DSM subtraction (Fig. 9a) suggests a retrogressive movement of the landslide crown from 2020 to 2021, characterized by a displacement from 0.5 up to 1 m. The area immediately below the 2014 source area showed an uprising of about 0.2–0.4 m, due to the accumulation of the loose material collapsed from the scarp. On the south-west side of the landslide, the DSM subtraction enlightens

the evolution of a new cracks system, formed at the beginning of 2020 and displaced about 1.2 m downward (Fig. 9b). This is one of the evidences of the landslide activity during the monitoring period, due to the scarp instability related to the landslide settling.

The landslide activity was confirmed also by the reinforced soil raising of about 0.5 m, probably due to the roto-translational displacement of the landslide (Fig. 9a).

Furthermore, the DSM subtraction highlighted the damages to the downslope buildings, immediately below the landslide, where collapses of about 5 m occurred (Fig. 9a).

Since profile curvatures are calculated parallel to the slope, the associated map was classified by using small values of standard deviation, in order to reveal the evidence of transverse structures with respect to the landslide slope. The analysis of profile curvatures confirmed the presence of the morphological step in the proximity of the forming cracks, with positive curvature angles (concavity) related to the presence of a fissure (Fig. 10).

Similar structures, with strongly positive curvature angles, were detected by the profile curvature analysis within the landslide scarp. It confirmed the temporal evolution of the landslide in terms of cracks formation, evolution, and collapse.

Profile curvatures detected also the area hosting debris material, immediately below the pile wall and well identified by infrared images (Fig. 10a-point 7).

On the other hand, the planar curvature, calculated perpendicular to the direction of the maximum slope, highlighted the presence of structures along the maximum slope lines, such as flow channels. These drain the runoff water from the landslide crown,

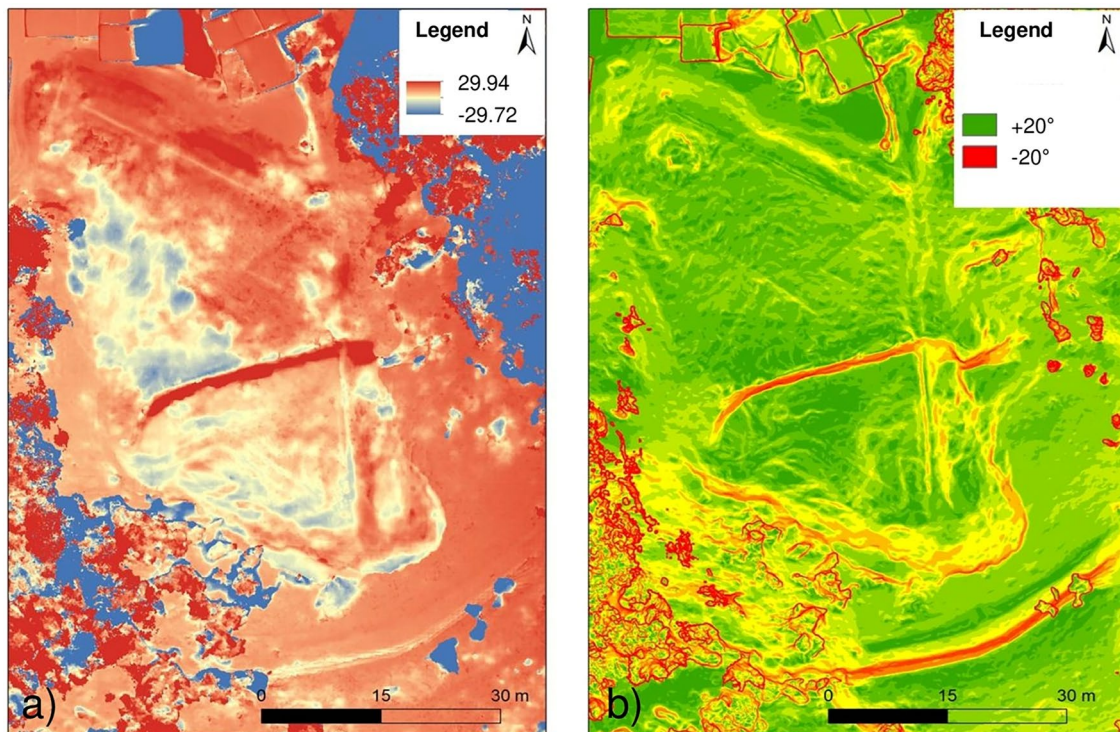


**Fig. 9** Morphometric analysis conducted on high resolution DSM. **a** Subtraction between DSM 2020 and DSM 2021 (values in m); **b** subtraction between slope angle 2020 and slope angle 2021 (values in °)

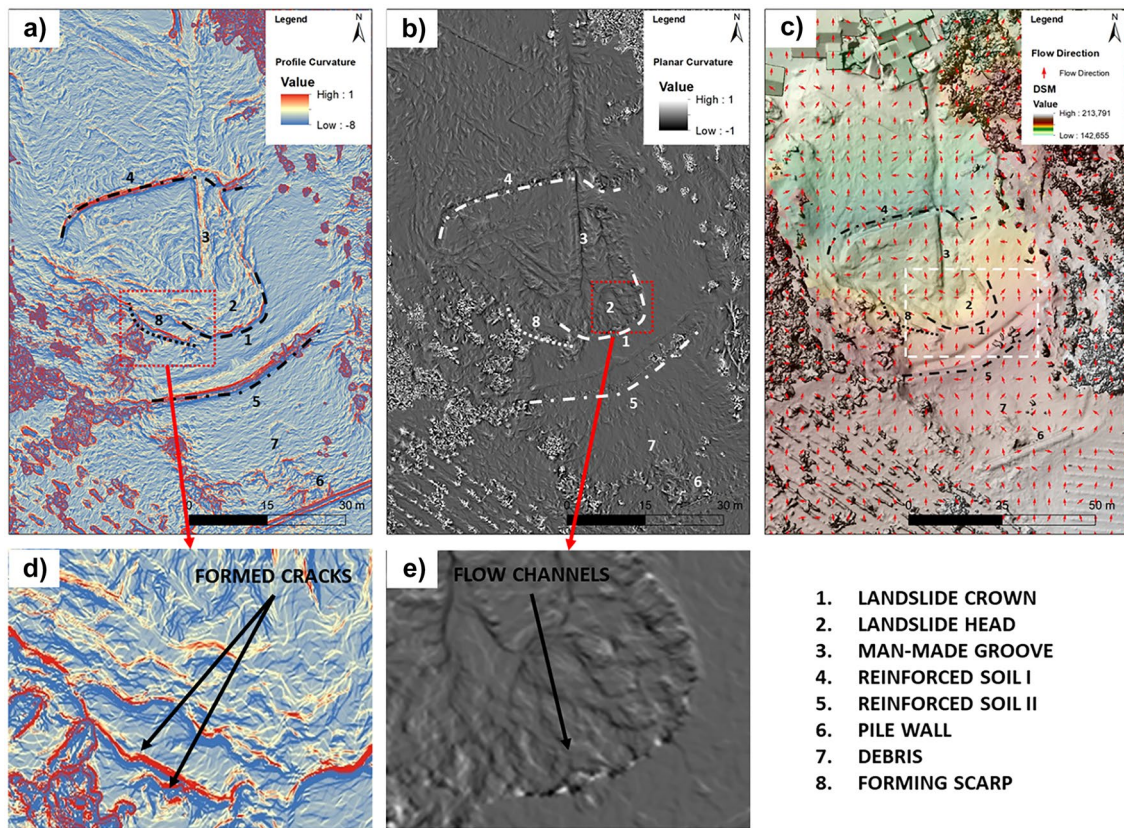


**Fig. 10** Morphometric analysis conducted on high resolution DSM: **a** profile curvature map classified in order to highlight transversal structures respect of the landslide slope; **b** planar curvature map stretched to made evident the perpendicular structures respect of the landslide slope, such as flow channel; **c** flow direction calculated

on the high resolution DSM shows the main directions around the landslide; **d** particular of profile curvature map in the area with the presence of cracks and new forming scarp; **e** particular of planar curvature map in the landslide area highlights the presence of a complex superficial drainage system

conveying water below the landslide scarp, also confirmed by the wet terrains detected by the thermal images acquired after a precipitation period (Fig. 7b).

The flow direction retrieved from DSM verified the modeled direction of water fluxes along the landslide scarp, transforming the surface of the landslide slope into a drainage system. This superficial drainage is also appreciable in the planar curvature map, revealing a complex drainage system from the head along the slope of the landslide.

### Analysis of thermal slope profiles

The qualitative analysis of thermograms highlighted that local anomalies of surface temperature are linked to specific features or elements occurring at the landslide area. With the aim of evaluating their quantitative incidence, so to shed light on a further innovative application of IRT on landslides, thermal slope profiles were drafted along representative cross section of the landslide and were compared to the morphological slope sections built from the DSMs previously defined by photogrammetric UAV data interpretation. Starting from the initial condition dating March 2021 (Fig. 11a), the thermal slope profile shows several positive peaks alternating to negative ones. Starting from ENE, the low ground surface

temperature is interrupted by a positive peak (n. 1) found at the thermal evidence of new developing cracks at the landslide side. This is followed by a second peak (n. 2) corresponding to the cracks between the main scarp and the mobilized material. The third peak deserving a comment (n. 3) is located at the western edge of the crown, where open cracks occur, followed by peak n. 4 occurring at the new formation scarp. On the other hand, negative anomalies affect the low plateau to the east (n. 5), which correspond to in-situ material still not visibly affected by movement, and the partly mobilized material on the opposite side (negative peak n. 6).

By analyzing the same profile drawn on the April thermogram (Fig. 11b), the peak n. 1 is still present at the new forming cracks. No quantitative comparison between peaks can be carried out herein, due to the different climate condition between the two survey campaigns, although interesting consideration can be proposed. In fact, the n. 5 plateau is herein replaced by a positive anomaly holding a new peak (n. 7), suggesting the presence of new forming secondary cracks in a partly mobilized material, thus a sort of evolution of the movement within 1 month. No appreciable differences are outlined for peak n. 2 in terms of location, although it is less evident probably due to the rainfalls occurred in the previous days. At peak 3, the morphological comparison between the topography of March and April testifies the occurrence of movements resulting in a slight

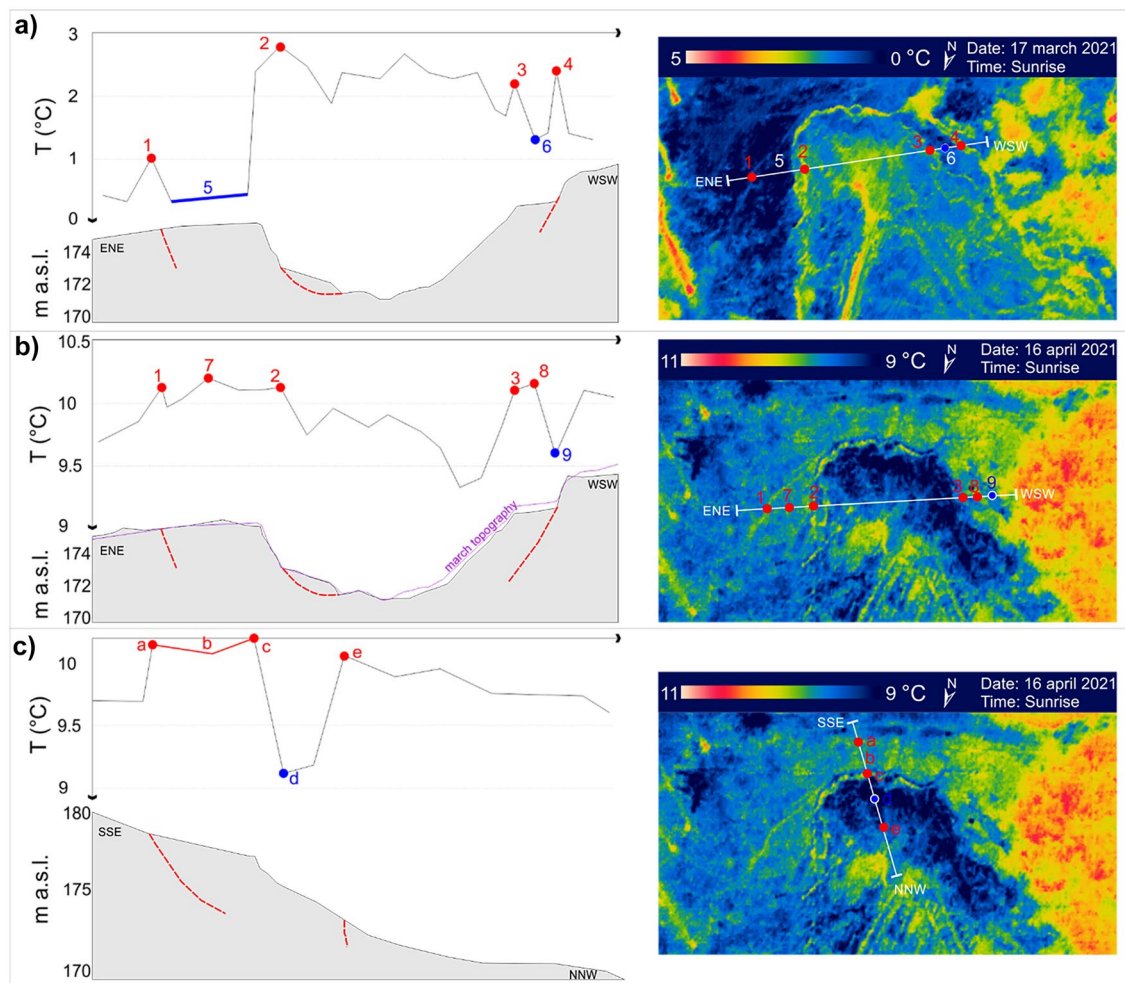


**Fig. 11** Thermal slope profiles and corresponding trace on thermogram for (a) 17 March survey ENE-WSW section; (b) 16 April survey ENE-WSW section; (c) 16 April survey SSE-NNW section

ground lowering. Here, the mobilized material is represented by positive anomalies culminating at peak n. 8, suggesting the presence of loose material bounded by a more and more defined scarp holding a low surface temperature.

The longitudinal cross-section considered herein (Fig. 11c) returned hints on the slope condition upstream of the crown, where the qualitative thermograms interpretation suggested the possibility of a retrogressive evolution. In this case, starting from south, the low surface temperature trend is interrupted by a positive peak (a) located exactly at the semicircular thermal anomaly potentially linked to a retrogression crown. From this point as far as the crown edge, a positive plateau suggests the presence of loose material, which is a likely condition in the frame of an active landslide movement. The negative anomaly at the main scarp, probably due to wet condition, is herein highlighted by the negative peak, with a trend interrupted by the positive peak e located at cracks surveyed at the lower portion of the main scarp.

All these considerations support the IRT evidence of an active movement evolving with a lateral component on both flanks and a retrogressive attitude.

## Discussion

Results achieved in this study pave the way to several discussion points focusing on the field validation of IRT data, the match between IRT and photogrammetric outcomes, and the methodological approach presented, in terms of potential and limitation.

## Discussion on results

The interpretation of IRT images suggests that open and partly open cracks are highlighted by positive anomalies (higher surface temperatures), which faithfully trace the crack development. This is in accordance with literature experiences focused on fractured rocks, both in field and in laboratory, reporting that there is a certain relationship between the crack aperture/persistence and its surface temperature, which is higher than the surrounding sound rock (e.g. Pappalardo et al. 2016; Pappalardo and Mineo 2017; Mineo et al. 2022). This outcome is, however, related to a specific environmental condition at the time of the survey, which is the absence of

direct solar radiation. In this specific time, indeed, the slope undergoes a cooling phase and cracks, along with hollow spots, represent parts preserved from cooling. Moreover, air circulating within the fracture network transports heat from the deep ground to the surface. In this process, warm air, which is lighter and more buoyant than the cold air, tends to rise through joints and cracks towards the surface. This process is well known to cavers, who commonly identify caves in rock slopes by looking for melted snow spots in winter (e.g. Rinker 1975; Baroň et al. 2014 and references therein). What was stated above was confirmed by a field data validation, which allowed ascertaining that peaks related to the highest surface temperatures along the thermal slope profiles correspond to cracks, in development during the monitored time spans, confirming the kinematic evolution of the slope movement. The new cracks were characterized by a quite continuous trend along their lines of development, testifying an enlargement and a partial retrogression of the landslide movements. These cracks were 0.4–1.1 m deep and formed mostly during the period between March and April 2021, according to field surveys and the analyses of both thermograms and DTMs. Moreover, the secondary peak (e in Fig. 11c) between 9.5 and 10 °C corresponds to an area with the presence of detensioning cracks, deep about 0.6–0.7 m b.g.l., and mostly with N-S direction, which could also favor the water drainage. Similarly, the significant negative peaks show a morphological correspondence (Figs. 12, 13). In fact, the area with lower surface temperatures at peaks n. 5, n. 6, and n. 9 is not significantly affected by both new high displacements and formation of new cracks. The lower surface temperature at these spots could be therefore due to the presence of moisture in the subsoil. The absence of cracks, in fact, could favor the sub-surficial water retention rather than its drainage, thus the increase of ground

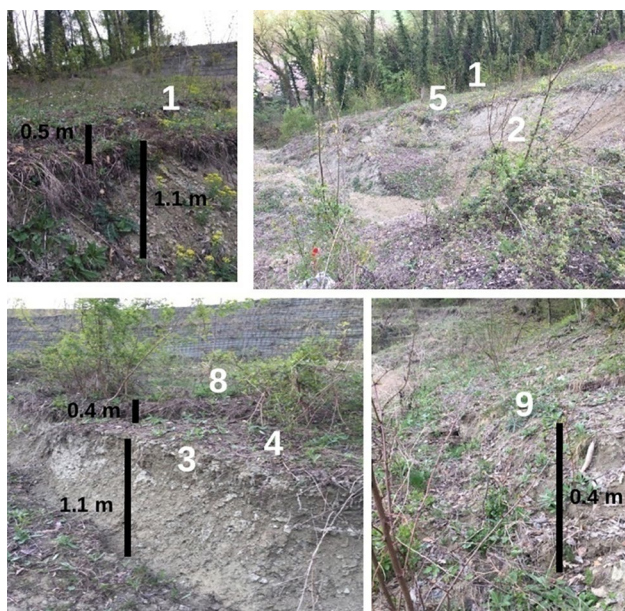


**Fig. 12** Morphological evidences on the unstable slope of the positive and negative thermal peaks identified along the analyzed transversal profiles of Fig. 11a and b. The numbers indicated in the images correspond to the peak numbers reported in the profiles of Fig. 11a and b

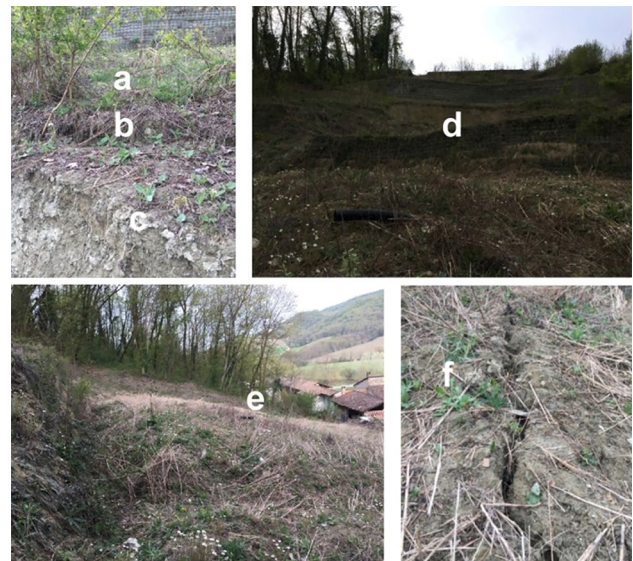


**Fig. 13** Morphological evidences on the unstable slope of the positive and negative thermal peaks identified along the analyzed longitudinal profile of Fig. 13c. The letters indicated in the images correspond as location to the ones presented in the profiles of Fig. 13c

humidity. This occurs also at the negative peak d, in the longitudinal profile of Fig. 11c, where a certain rate of ground humidity was detected by field surveys. In the landslide area, mainly characterized by soil affected by displacement, there is no remarkable thermal contrast between soil and vegetation, which allows a good definition of the thermal anomalies arising from the landslide elements. The area where vegetation was taken as a marker of loose material is at the pile wall (Fig. 7), where IRT allowed delimiting the debris accumulation by exploiting the thermal contrast between soil and vegetation. These considerations, although qualitative, strengthen the potential of IRT technique applied to slope stability problems and can be further discussed on a combined DSM-IRT model, which provides a useful tool to better understand and percept the achieved results (Fig. 14). More specifically, the model related to the March surveying campaign (Fig. 14a) shows how the positive anomalies at the eastern landslide flank are likely related to open cracks, while the forming scarp on the opposite side is characterized by an already defined plane highlighted by a warmer surface temperature. The presence of this new-forming scarp, located few meters upwards the main scarp, suggests that the movement is in progress. Moreover, signs of open cracks are present along the main scarp, with specific reference to the western sector, labeled by linear anomalies. The slightly open crack on the eastern flank, likely related to a future enlargement of the landslide, is well recognizable and its junction with the main crown suggests the active state of the landslide itself. Furthermore, a detail that could have been missed in the 2D thermogram analysis, due to the absence of perspective, is the circular cold area located at the upper part of the main crown, whose shape and position did not change during the thermal monitoring (Fig. 14b). This feature could be related to the drainage network accomplished in the past mitigation works, thus representing a potential hydraulic vent. This is corroborated by the evidence of water circulation in the April thermogram (Fig. 14b), which was taken after some rainfall

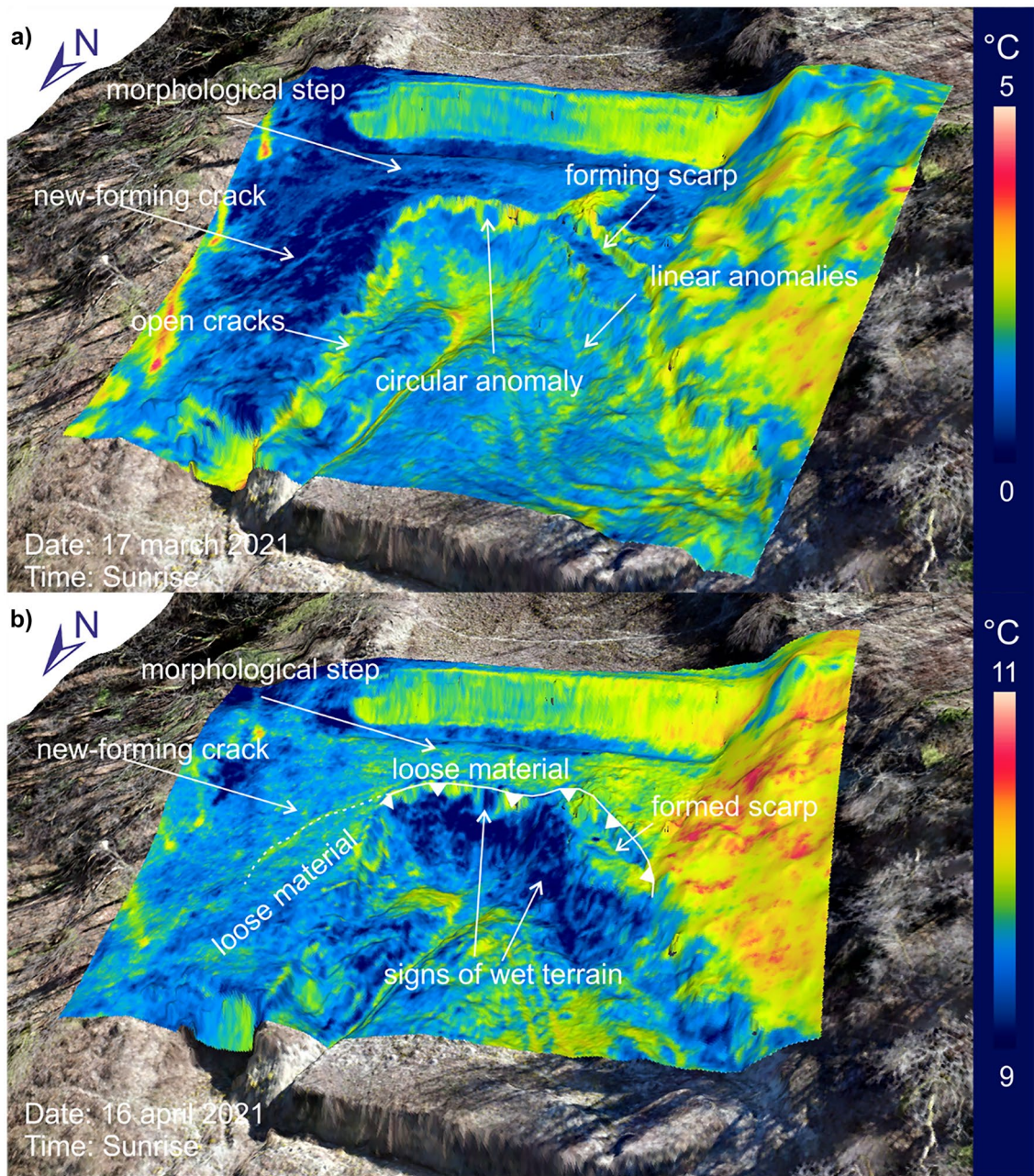


**Fig. 14** DSM-IRT model of the landslide referring to the March (a) and April (b) surveying campaigns

days. With reference to the April model, the western forming scarp appears well developed and labeled by a cold surface temperature, unlike how it looked in March. This is likely due to both a different field setting arising from ground movements, as confirmed by the topographic monitoring, and to the different climate condition between the previous surveying campaign. At this stage, the scarp is well exposed and its junction with the main scarp is defined, suggesting the boundary of the enlarging landslide sector. Finally, the slight morphological step upstream the main crown can be identified, thus representing a key warning signal of potential retrogression of the movement.

#### Discussion on the methodological approach

Presented results demonstrate that the integrated airborne photogrammetry and IRT provide a reliable tool for non-contact, quick, and versatile surveys covering wide areas, even if affected by a poor logistics in terms of access and field campaigns. The usefulness of UAV surveys is known in literature (e.g. Chudý et al. 2019; Conforti et al. 2020; Giordan et al. 2020; Godone et al. 2020; Liu et al. 2021; Mineo et al. 2021; Nappo et al. 2021; Peppia et al. 2017; Peternel et al. 2017; Rossi et al. 2018; Turner et al. 2015), as well as the integration of IRT with other remote surveying methods (e.g. Casagli et al.

2017; Frodella et al. 2020; Pappalardo et al. 2021; Grechi et al. 2021; Mineo et al. 2022); nevertheless, the case presented herein provides the opportunity to match multitemporal and multisensor information acquired by the same aerial surveying perspective. This allows overcoming some limitations arising from the interpretation of data acquired by different perspectives, which is common when dealing with the integration of terrestrial IRT and other remote surveying techniques. This aspect is crucial during slope monitoring, when IRT is expected to detect even feeble signs of instability, which have to be located with accuracy on a digital model of the slope for practical applications. In fact, in this study, the same ground control points were used for both RGB and IRT photogrammetry, leading to a precise match between outcomes. On the other hand, a limiting aspect is that the best condition for IRT surveys applied to slope instability is the environmental dark (from sunset to sunrise), when the contribution of parasite radiation is low. This aspect, already suggested by other studies in literature (Pappalardo and Mineo 2019) and herein strengthened, forces to split the RGB and IRT surveys in different times of the day. RGB image acquisition should be carried out in daylight, while IRT survey should be performed either late in the afternoon or early in the morning, so to have a residual natural lighting for ground operation related to the UAV piloting and data acquisition.

Another discussion point is that IRT data further proved reliable and useful in detecting key instability features, such as forming cracks, loose material, and presence of water, in accordance to other literature experiences (e.g. Teza et al. 2012; Mineo et al. 2015; Casagli et al. 2017). This advantage gains significance for the survey of wide areas, where the location of such elements is time consuming and conditioned by the expertise of surveyors. Moreover, the novelty brought by this research is the successful tentative of correlating the slope instability features detected by IRT with the surface temperature trend measured along some profiles crossing the landslide areas. Such thermal slope profiles provide the advantage of a quick and intuitive location of the aforementioned key elements. This practice can be addressed as a pioneering useful procedure supporting the qualitative analysis of thermal images, paving the way to interesting applications even on other types of landslides. Nevertheless, a possible limitation of this approach could arise for surveys of landslides characterized by a complex slope surface morphology, as well as by abundant mobilized material, which could suffer from a lower accuracy in the recognition of key thermal anomalies. This aspect underlines the need for further studies aimed at testing such methodological approach on different contexts. Finally, it must be underlined that the still limited experience in literature in the use of IRT for landslide monitoring, although in growing progress, implied a certain degree of caution and the need of validating achieved results by field surveys. In this research, validation outcomes were successful, as all the conclusions achieved by the integrated airborne methods found a positive feedback in the field, suggesting the great potential of such remote surveying approach, which surely deserves further tests on different geological settings to be implemented.

## Conclusions

This research was aimed at shedding light on a novel application of combined remote surveying technologies applied to landslide monitoring. Airborne RGB and IRT photogrammetry was used herein to

study and monitor a complex landslide occurred in the Oltrepò Pavese hilly zone (northwestern Italy), which suffered multiple reactivation stages even after important stabilization works. The application of such remote surveying techniques allowed to draw key conclusions on the state and distribution of activity of the studied movement, which is affected by a retrogressive and enlargement trend according to monitoring data referring to three campaigns carried out after the last greatest reactivation. According to achieved results, the conclusions of this research can be summarized as follows:

1. Aerial IRT allows detecting key features along a wide unstable slope portion, based on the thermal contrast occurring between cracks, loose material, wet ground, and the surrounding environment.
2. Thermal slope profiles built along specific sections crossing the landslide allow achieving a good definition of the main features involved in the instability process. This represents a useful quantitative approach supporting the qualitative analysis of post-processed thermal images.
3. The comparison between DSM built after different campaigns allowed highlighting the presence of landslide activities, as well as mapping the evolution of new cracks and the damages to buildings affected by the mass movement.
4. RGB photogrammetry and IRT represent two reliable remote surveying methodologies, which, if combined, can lead to the definition of useful landslide models with interesting hints also on the actual and/or potential evolution.

## Acknowledgements

The Authors thank the Editor and the anonymous Reviewers for their support and constructive comments.

## Funding

Open access funding provided by Università degli Studi di Catania within the CRUI-CARE Agreement. The work was developed in the frame of the research contract between Borgo Priolo municipality and the Department of Earth and Environmental Sciences of University of Pavia, entitled “Geological, geomorphological, hydrogeological and geological-technical study of the hillslope above the village of Ghiaia dei Risi”, fund recipients Claudia Meisina and Massimiliano Bordoni. The analysis of thermal images was carried out under the financial support of University of Catania in the frame of projects: “CH2V – Cultural Heritage Hazard and Vulnerability” Piaceri linea 2, PI Giovanna Pappalardo, and “MODellazione Digitale di fenomeni di Instabilità di Versante attraverso procedure di telerilevamento MODIV” Piaceri linea 3 Starting Grant, PI Simone Mineo.

## Declarations

**Conflict of interest** The authors declare no competing interests.

**Open Access** This article is licensed under a Creative Commons Attribution 4.0 International License, which permits use, sharing, adaptation, distribution and reproduction in any medium or format, as long as you give appropriate credit to the original author(s) and the source, provide a link to the Creative Commons licence,

and indicate if changes were made. The images or other third party material in this article are included in the article's Creative Commons licence, unless indicated otherwise in a credit line to the material. If material is not included in the article's Creative Commons licence and your intended use is not permitted by statutory regulation or exceeds the permitted use, you will need to obtain permission directly from the copyright holder. To view a copy of this licence, visit <http://creativecommons.org/licenses/by/4.0/>.

## References

- Alfieri L, Salamon P, Pappenberger F et al (2012) Operational early warning systems for water-related hazards in Europe. *Environ Sci Policy* 21:35–49. <https://doi.org/10.1016/j.envsci.2012.01.008>
- Barla G, Antolini F, Gigli G (2016) 3D Laser scanner and thermography for tunnel discontinuity mapping. *Geomech Tunn* 9:29–36. <https://doi.org/10.1002/geot.201500050>
- Baroň I, Bečkovský D, Míča L (2014) Application of infrared thermography for mapping open fractures in deep-seated rockslides and unstable cliffs. *Landslides* 11:15–27. <https://doi.org/10.1007/s10346-012-0367-z>
- Bianchini S, Solari L, Bertolo D et al (2021) Integration of satellite interferometric data in civil protection strategies for landslide studies at a regional scale. *Remote Sens* 13:1881. <https://doi.org/10.3390/rs13101881>
- Boni R, Bordoni M, Vivaldi V et al (2020) Assessment of the Sentinel-1 based ground motion data feasibility for large scale landslide monitoring. *Landslides* 17:2287–2299. <https://doi.org/10.1007/s10346-020-01433-3>
- Bordoni M, Vivaldi V, Lucchelli L et al (2021) Development of a data-driven model for spatial and temporal shallow landslide probability of occurrence at catchment scale. *Landslides* 18:1209–1229. <https://doi.org/10.1007/s10346-020-01592-3>
- Canuti P, Casagli N, Ermini L et al (2004) Landslide activity as a geoinicator in Italy: significance and new perspectives from remote sensing. *Environ Geol* 45:907–919. <https://doi.org/10.1007/s00254-003-0952-5>
- Casagli N, Frodella W, Morelli S et al (2017) Spaceborne, UAV and ground-based remote sensing techniques for landslide mapping, monitoring and early warning. *Geoenvironmental Disasters* 4:9. <https://doi.org/10.1186/s40677-017-0073-1>
- Cascini L, Calvello M, Grimaldi GM (2014) Displacement trends of slow-moving landslides: Classification and forecasting. *J Mt Sci* 11:592–606. <https://doi.org/10.1007/s11629-013-2961-5>
- Chae B-G, Park H-J, Catani F et al (2017) Landslide prediction, monitoring and early warning: a concise review of state-of-the-art. *Geosci J* 21:1033–1070. <https://doi.org/10.1007/s12303-017-0034-4>
- Chudý F, Slámová M, Tomašík J et al (2019) Identification of micro-scale landforms of landslides using precise digital elevation models. *Geosciences* 9:117. <https://doi.org/10.3390/geosciences9030117>
- Colomina I, Molina P (2014) Unmanned aerial systems for photogrammetry and remote sensing: a review. *ISPRS J Photogramm Remote Sens* 92:79–97. <https://doi.org/10.1016/j.isprsjprs.2014.02.013>
- Conforti M, Mercuri M, Borrelli L (2020) Morphological changes detection of a large earthflow using archived images, LiDAR-derived DTM, and UAV-based remote sensing. *Remote Sens* 13:120. <https://doi.org/10.3390/rs13010120>
- Corominas J, van Westen C, Frattini P et al (2013) Recommendations for the quantitative analysis of landslide risk. *Bull Eng Geol Environ*. <https://doi.org/10.1007/s10064-013-0538-8>
- Crosta GB, Agliardi F, Rivolta C et al (2017) Long-term evolution and early warning strategies for complex rockslides by real-time monitoring. *Landslides* 14:1615–1632. <https://doi.org/10.1007/s10346-017-0817-8>
- Crosta GB, di Prisco C, Frattini P et al (2014) Chasing a complete understanding of the triggering mechanisms of a large rapidly evolving rockslide. *Landslides* 11:747–764. <https://doi.org/10.1007/s10346-013-0433-1>
- Cruden DM, Varnes DJ (1996) *Landslide Types and Processes*, Transportation Research Board, U.S. National Academy of Sciences, Special Report 247:36–75
- DeWitt DP, Nutter GD (eds) (1988) *Theory and practice of radiation thermometry*. Wiley, New York
- Ferretti A, Prati C, Rocca F (2001) Permanent scatterers in SAR interferometry. *IEEE Trans Geosci Remote Sens* 39:8–20. <https://doi.org/10.1109/36.898661>
- FLIR. User's Manual FLIR T6xx Series (2017) Available online: <https://www.flir.com/globalassets/imported-assets/document/flir-t6xx-series-user-manual.pdf>. Accessed 12 September 2022
- Fiorucci M, Marmoni GM, Martino S, Mazzanti P (2018) Thermal response of jointed rock masses inferred from infrared thermographic surveying (Acuto Test-Site, Italy). *Sensors* 18:2221. <https://doi.org/10.3390/s18072221>
- Frodella W, Elashvili M, Spizzichino D et al (2020) Combining infrared thermography and UAV digital photogrammetry for the protection and conservation of rupestrian cultural heritage sites in Georgia: a methodological application. *Remote Sens* 12:892. <https://doi.org/10.3390/rs12050892>
- Froude MJ, Petley DN (2018) Global fatal landslide occurrence from 2004 to 2016. *Nat Hazards Earth Syst Sci* 18:2161–2181. <https://doi.org/10.5194/nhess-18-2161-2018>
- Fusco F, Bordoni M, Tufano R et al (2022) Hydrological regimes in different slope environments and implications on rainfall thresholds triggering shallow landslides. *Nat Hazards*. <https://doi.org/10.1007/s11069-022-05417-5>
- Garnica-Peña RJ, Alcántara-Ayala I (2021) The use of UAVs for landslide disaster risk research and disaster risk management: a literature review. *J Mt Sci* 18:482–498. <https://doi.org/10.1007/s11629-020-6467-7>
- Giordan D, Adams MS, Aicardi I et al (2020) The use of unmanned aerial vehicles (UAVs) for engineering geology applications. *Bull Eng Geol Environ* 79:3437–3481. <https://doi.org/10.1007/s10064-020-01766-2>
- Giordan D, Hayakawa Y, Nex F et al (2018) Review article: the use of remotely piloted aircraft systems (RPASs) for natural hazards monitoring and management. *Nat Hazards Earth Syst Sci* 18:1079–1096. <https://doi.org/10.5194/nhess-18-1079-2018>
- Giordan D, Manconi A, Remondino F, Nex F (2017) Use of unmanned aerial vehicles in monitoring application and management of natural hazards. *Geomat Nat Hazards Risk* 8:1–4. <https://doi.org/10.1080/19475705.2017.1315619>
- Godone D, Allasia P, Borrelli L, Gullà G (2020) UAV and structure from motion approach to monitor the maierato landslide evolution. *Remote Sens* 12:1039. <https://doi.org/10.3390/rs12061039>
- Grechi G, Fiorucci M, Marmoni GM, Martino S (2021) 3D thermal monitoring of jointed rock masses through infrared thermography and photogrammetry. *Remote Sens* 13:957. <https://doi.org/10.3390/rs13050957>
- Guerin A, Jaboyedoff M, Collins BD et al (2019) Detection of rock bridges by infrared thermal imaging and modeling. *Sci Rep* 9:13138. <https://doi.org/10.1038/s41598-019-49336-1>
- Guo Z, Yin K, Gui L et al (2019) Regional rainfall warning system for landslides with creep deformation in three gorges using a statistical black box model. *Sci Rep* 9:8962. <https://doi.org/10.1038/s41598-019-45403-9>
- Guzzetti F, Gariano SL, Peruccacci S et al (2020) Geographical landslide early warning systems. *Earth-Sci Rev* 200. <https://doi.org/10.1016/j.earscirev.2019.102973>
- Havens KJ, Sharp EJ (2016) *Thermal imaging techniques to survey and monitor animals in the wild: a methodology*. Elsevier/Academic Press, Amsterdam, Boston
- Herrera G, Gutiérrez F, García-Davalillo JC et al (2013) Multi-sensor advanced DInSAR monitoring of very slow landslides: the Tena Valley case study (Central Spanish Pyrenees). *Remote Sens Environ* 128:31–43. <https://doi.org/10.1016/j.rse.2012.09.020>
- Hillel D (1998) *Environmental soil physics*. Academic Press, San Diego, CA
- Intrieri E, Carlà T, Gigli G (2019) Forecasting the time of failure of landslides at slope-scale: a literature review. *Earth-Sci Rev* 193:333–349. <https://doi.org/10.1016/j.earscirev.2019.03.019>
- Keefer DK, Wilson RC, Mark RK et al (1987) Real-time landslide warning during heavy rainfall. *Science* 238:921–925. <https://doi.org/10.1126/science.238.4829.921>



- Li C, Zhang G, Lei T, Gong A (2011) Quick image-processing method of UAV without control points data in earthquake disaster area. *Trans Nonferrous Met Soc China* 21:s523–s528. [https://doi.org/10.1016/S1003-6326\(12\)61635-5](https://doi.org/10.1016/S1003-6326(12)61635-5)
- Liu B, He K, Han M et al (2021) Application of UAV and GB-SAR in mechanism research and monitoring of Zhonghaicun landslide in Southwest China. *Remote Sens* 13:1653. <https://doi.org/10.3390/rs13091653>
- Liu D, Hu X, Zhou C et al (2020) Model test study of a landslide stabilized with piles and evolutionary stage identification based on thermal infrared temperature analysis. *Landslides* 17:1393–1404. <https://doi.org/10.1007/s10346-020-01355-0>
- Luo Y, Jiang W, Li B et al (2020) Analyzing the formation mechanism of the Xuyong landslide, Sichuan province, China, and emergency monitoring based on multiple remote sensing platform techniques. *Geomat Nat Hazards Risk* 11:654–677. <https://doi.org/10.1080/19475705.2020.1745903>
- Meisina C, Zucca F, Fossati D et al (2006) Ground deformation monitoring by using the permanent scatterers technique: the example of the Oltrepo Pavese (Lombardia, Italy). *Eng Geol* 88:240–259. <https://doi.org/10.1016/j.enggeo.2006.09.010>
- Meisina C, Zucca F, Notti D et al (2008) Geological interpretation of PSInSAR data at regional scale. *Sensors* 8:7469–7492. <https://doi.org/10.3390/s8117469>
- Melis M, Da Pelo S, Erbi I et al (2020) Thermal remote sensing from UAVs: a review on methods in coastal cliffs prone to landslides. *Remote Sens* 12:1971. <https://doi.org/10.3390/rs12121971>
- Mineo S, Caliò D, Pappalardo G (2022) UAV-based photogrammetry and infrared thermography applied to rock mass survey for geomechanical purposes. *Remote Sens* 14:473. <https://doi.org/10.3390/rs14030473>
- Mineo S, Pappalardo G, Onorato S (2021) Geomechanical characterization of a rock cliff hosting a cultural heritage through ground and UAV rock mass surveys for its sustainable fruition. *Sustainability* 13:924. <https://doi.org/10.3390/su13020924>
- Mineo S, Pappalardo G, Rapisarda F et al (2015) Integrated geospatial, seismic and infrared thermography surveys for the study of an unstable rock slope in the Peloritani Chain (NE Sicily). *Eng Geol* 195:225–235. <https://doi.org/10.1016/j.enggeo.2015.06.010>
- Nappo N, Mavrouli O, Nex F et al (2021) Use of UAV-based photogrammetry products for semi-automatic detection and classification of asphalt road damage in landslide-affected areas. *Eng Geol* 294. <https://doi.org/10.1016/j.enggeo.2021.106363>
- Ortiz-Sanz J, Gil-Docampo M, Arza-García M, Cañas-Guerrero I (2019) IR thermography from UAVs to monitor thermal anomalies in the envelopes of traditional wine cellars: field test. *Remote Sens* 11:1424. <https://doi.org/10.3390/rs11121424>
- Pappalardo G, Mineo S (2017) Investigation on the mechanical attitude of basaltic rocks from Mount Etna through infrared thermography and laboratory tests. *Constr Build Mater* 134:228–235. <https://doi.org/10.1016/j.conbuildmat.2016.12.146>
- Pappalardo G, Mineo S (2019) Study of jointed and weathered rock slopes through the innovative approach of infrared thermography. In: Pradhan SP, Vishal V, Singh TN (eds) *Landslides: Theory, Practice and Modelling*. Springer International Publishing, Cham, pp 85–103
- Pappalardo G, Mineo S, Angrisani AC et al (2018) Combining field data with infrared thermography and DInSAR surveys to evaluate the activity of landslides: the case study of Randazzo Landslide (NE Sicily). *Landslides* 15:2173–2193. <https://doi.org/10.1007/s10346-018-1026-9>
- Pappalardo G, Mineo S, Carbone S et al (2021) Preliminary recognition of geohazards at the natural reserve “Lachea Islet and Cyclop Rocks” (Southern Italy). *Sustainability* 13:1082. <https://doi.org/10.3390/su13031082>
- Pappalardo G, Mineo S, Imposa S et al (2020) A quick combined approach for the characterization of a cliff during a post-rockfall emergency. *Landslides* 17:1063–1081. <https://doi.org/10.1007/s10346-019-01338-w>
- Pappalardo G, Mineo S, Zampelli SP et al (2016) Infrared thermography proposed for the estimation of the Cooling Rate Index in the remote survey of rock masses. *Int J Rock Mech Min Sci* 83:182–196. <https://doi.org/10.1016/j.ijrmms.2016.01.010>
- Pecoraro G, Calvello M, Piciullo L (2019) Monitoring strategies for local landslide early warning systems. *Landslides* 16:213–231. <https://doi.org/10.1007/s10346-018-1068-z>
- Peduto D, Ferlisi S, Nicodemo G et al (2017) Empirical fragility and vulnerability curves for buildings exposed to slow-moving landslides at medium and large scales. *Landslides* 14:1993–2007. <https://doi.org/10.1007/s10346-017-0826-7>
- Peppia MV, Mills JP, Moore P et al (2017) Brief communication: landslide motion from cross correlation of UAV-derived morphological attributes. *Nat Hazards Earth Syst Sci* 17:2143–2150. <https://doi.org/10.5194/nhess-17-2143-2017>
- Peternel T, Kumej S, Oštir K, Komac M (2017) Monitoring the Potoška planina landslide (NW Slovenia) using UAV photogrammetry and tachymetric measurements. *Landslides* 14:395–406. <https://doi.org/10.1007/s10346-016-0759-6>
- Petley DN, Bulmer MH, Murphy W (2002) Patterns of movement in rotational and translational landslides. *Geology* 30:719. [https://doi.org/10.1130/0091-7613\(2002\)030<0719:POMIRA>2.0.CO;2](https://doi.org/10.1130/0091-7613(2002)030<0719:POMIRA>2.0.CO;2)
- Plank S, Singer J, Minet C, Thuro K (2012) Pre-survey suitability evaluation of the differential synthetic aperture radar interferometry method for landslide monitoring. *Int J Remote Sens* 33:6623–6637. <https://doi.org/10.1080/01431161.2012.693646>
- Prestinini A, Bianchi-Fasani G, Bozzano F et al (2013) From the refinement of geological models to risk management: the role of landslide monitoring. 6
- Raspini F, Bianchini S, Ciampalini A et al (2018) Continuous, semi-automatic monitoring of ground deformation using Sentinel-1 satellites. *Sci Rep* 8:7253. <https://doi.org/10.1038/s41598-018-25369-w>
- Rinker JN (1975) Airborne infrared thermal detection of caves and crevasses. *Photogramm Eng* 10
- Rossi G, Tanteri L, Tofani V et al (2018) Multitemporal UAV surveys for landslide mapping and characterization. *Landslides* 15:1045–1052. <https://doi.org/10.1007/s10346-018-0978-0>
- Solari L, Del Soldato M, Montalti R et al (2019) A Sentinel-1 based hotspot analysis: landslide mapping in north-western Italy. *Int J Remote Sens* 40:7898–7921. <https://doi.org/10.1080/01431161.2019.1607612>
- Teza G, Marcato G, Castelli E, Galgaro A (2012) IRTROCK: A MATLAB toolbox for contactless recognition of surface and shallow weakness of a rock cliff by infrared thermography. *Comput Geosci* 45:109–118. <https://doi.org/10.1016/j.cageo.2011.10.022>
- Turner D, Lucieer A, de Jong S (2015) Time series analysis of landslide dynamics using an unmanned aerial vehicle (UAV). *Remote Sens* 7:1736–1757. <https://doi.org/10.3390/rs70201736>
- Vallet A, Varron D, Bertrand C et al (2016) A multi-dimensional statistical rainfall threshold for deep landslides based on groundwater recharge and support vector machines. *Nat Hazards* 84:821–849. <https://doi.org/10.1007/s11069-016-2453-3>
- Westoby MJ, Brasington J, Glasser NF et al (2012) ‘Structure-from-Motion’ photogrammetry: a low-cost, effective tool for geoscience applications. *Geomorphology* 179:300–314. <https://doi.org/10.1016/j.geomorph.2012.08.021>
- Wu S, Hu X, Zheng W et al (2021) Threshold definition for monitoring Gapa landslide under large variations in reservoir level using GNSS. *Remote Sens* 13:4977. <https://doi.org/10.3390/rs13244977>
- Xia H, Hu X, Tang H et al (2017) Rock and soil mechanics. *Appl Infrared Therm Radiat Imaging Technol Landslide Phys Model Test* 38. <https://doi.org/10.16285/j.rsm.2017.01.037>
- Yin Y, Wang H, Gao Y, Li X (2010) Real-time monitoring and early warning of landslides at relocated Wushan Town, the Three Gorges Reservoir, China. *Landslides* 7:339–349. <https://doi.org/10.1007/s10346-010-0220-1>

**V. Vivaldi · M. Bordoni · M. Crozi · C. Meisina**

Dipartimento Di Scienze Della Terra E Dell’Ambiente, Università Degli Studi Di Pavia, Via Adolfo Ferrata 7, 27100 Pavia, Italy

**S. Mineo** (✉) · **G. Pappalardo**

Dipartimento Di Scienze Biologiche, Geologiche E Ambientali, Università Degli Studi Di Catania, Corso Italia 57, 95129 Catania, Italy  
Email: smineo@unic.it